Available online at www.sciencedirect.com
SCIENCE DIRECT®
Sensors and Actuators A 107 (2003) 248–260
SENSORS AND ACTUATORS A PHYSICAL
www.elsevier.com/locate/sna

Design of bimorph piezo-composite actuators with functionally graded microstructure

Minoru Taya [a,*], Abdulhakim A. Almajid [b], Martin Dunn [c], Hirofumi Takahashi [d]

[a] *Department of Mechanical Engineering, Center for Intelligent Materials and Systems, University of Washington, Box 352600, Seattle, WA 98195-2600, USA*
[b] *Department of Mechanical Engineering, King Saud University, P.O. Box 800, Riyadh 11421, Saudi Arabia*
[c] *Department of Mechanical Engineering, University of Colorado, Boulder, CO 80309-0427, USA*
[d] *Fuji Ceramics Corporation, 2320-11 Yamamiya, Fujinomiya City, Shizuoka Prefecture 418-0111, Japan*

Received 27 January 2003; received in revised form 10 June 2003; accepted 3 July 2003

Abstract

Piezoelectric actuators with functionally graded microstructure (FGM) are designed with the aim of reducing the stress concentration at the middle interface that exists in the standard bimorph actuators while maintaining high bending displacement. A FGM piezoelectric laminate consists of a number laminae, which are composite materials with electroelastic properties varied through the laminate thickness. The electroelastic behavior of piezo-actuators with laminated composite is studied by two-stage hierarchical model, the first based on the Eshelby's model for predictions of the electroelastic properties of each lamina, the second based on classical lamination theory (CLT). The in-plane stresses and out-of-plane displacements are obtained by the CLT for both standard and FGM piezoelectric bimorph actuators under the assumption of cylindrical bending. The microstructure of the FGM biomorph actuator is optimized by using CLT model to achieve the best performance of the FGM piezoelectric actuator, i.e. large bending displacement while minimizing the induced stress field. Based on the optimized microstructure of the FGM bimorph actuators by the CLT model, we processed the FGM bimorph actuator that is composed of six laminae, and also the standard bimorph actuator. The bending displacements of these actuators are then measured by a laser displacement measurement apparatus as a function of applied voltage. The measured data of the bending displacements versus applied voltage are compared with the predictions by the CLT, resulting in a good agreement.

Keywords: Piezoelectric; Bimorph actuator; Functionally gradient microstructure; Composite; Modeling

1. Introduction

Piezoelectric materials have been used extensively in the design of sensors and actuators. Several designs of piezoelectric actuators have been investigated. Uchino et al. fabricated a monomorph made from semiconductive piezoelectric ceramics [1]. A rainbow type actuator was developed by Haertling [2] by reducing one surface of a PZT wafer that creates a non-uniform electric field when voltage is applied. Wu et al. [3] fabricated a piezoelectric actuator where the electrical resistivity was graded through the plate thickness leading to a graded poling of the material. Piezoelectric bimorph produces high bending displacement at cost of high stress concentration at the interface between the top and bottom layers, reducing its lifetime [4]. The use of epoxy resin to bond the top and bottom layers in the bimorph piezoelectric actuator made the interface fragile and fatigue prone [5]. Zhu and Meng [6] and Zhu et al. [6,7] designed the piezoelectric bending actuators with functionally graded microstructure (FGM) where the top layer has high dielectric constant and low piezoelectric constant, the bottom layer has the opposite properties, and the mid-layer is graded smoothly across the thickness. In order to reduce high stress concentration at the mid-interface, the concept of functionally graded microstructure is introduced, where a piezo-actuator of bimorph type is composed of a number of laminae with each being a piezoelectric composite, and the electroelastic properties of laminae are graded through the thickness direction such that the mirror symmetry with respect to the mid-plane is maintained. In order to identify the optimum microstructure of FGM piezo laminated composite, we shall use two-stage modeling (1) homogenization of each FGM layer (lamina) based on the Eshelby's model [8–10] and (2) the classical laminate theory (CLT) devel-

* Corresponding author. Tel.: +1-206-685-2850; fax: +1-206-685-8047.
E-mail address: tayam@u.washington.edu (M. Taya).

0924-4247/$ – see front matter © 2003 Published by Elsevier B.V.
doi:10.1016/S0924-4247(03)00381-9

oped by Almajid et al. [11]. The accuracy of CLT solutions will be checked against those based on elasticity model [12] and the finite element method (FEM). In the following sections, we shall discuss the homogenization modeling using Eshelby's model in Section 2, and classical lamination theory (CLT) in Section 3. The results of the electroelastic properties of each lamina calculated by the Eshelby's model is given in Section 4. Design optimization of piezo laminated composite actuators is given in Section 5. Then, we processed both standard bimorph and FGM bimorph actuators by plasma sintering, semi-details of which are described in Section 6. Finally, experimental evaluation of the out-of-plane displacements of the piezo-actuator for both standard bimorph and FGM bimorph types and their results compared with the analytical predictions are discussed in Section 6, followed by conclusion in Section 7.

2. Modeling of piezoelectric composites

A piezoelectric composite is normally composed of several different piezoelectric materials resulting from the combination of piezoelectric materials with piezo or non-piezo-materials. Examples of a piezoelectric composite include piezoelectric ceramic rods or particles embedded in a polymer matrix, and porous piezoelectric ceramics. The combination of piezoelectric rods embedded in a polymer matrix has been shown to result in piezoelectric performance that exceeds even that of piezoelectric ceramics [13].

The development of piezoelectric composites has its roots in the early work of Newham et al. [14]. Newham lays out a terminology used to describe the microstructure of piezoelectric composites in terms of their connectivity, where a two-phase composite is denoted by X–Y system and X and Y refer to the connectivity of the piezoelectric and non-piezoelectric phases, respectively. By this definition, 0–3 and 3–0 composites denote polymers reinforced by piezoelectric particles, and voided piezoelectric ceramics or polymers. Composites of 1–3 and 3–1 connectivity are often fabricated by embedding continuous piezoelectric rods in a polymer matrix or by boring holes in a solid piezoelectric ceramic and impregnating them with a soft polymer. Newham and coworkers [14,15] forwarded the understanding of the physical behavior of piezoelectric composite through the development of *mechanics-of-materials* type parallel and series models. This understanding, particularly of 1–3 composites, was significantly enhanced by Smith and coworkers [13,16–19] in the analysis of continuous fiber-reinforced piezoelectric composites. In these approaches, a simplifying assumption of either a constant stress or strain component in the composite has been made which then leads to the application of Voigt and Reuss type estimates. More recent developments in the modeling of piezoelectric composites based on rigorous micromechanics modeling are made by Dunn and coworkers [8–10]. These include the dilute, self-consistent, Mori–Tanaka (MT), and differential scheme models. The key to each of these methods is the use of the stress and strain concentration factor tensors obtained through the solution of a single particle embedded in an infinite medium, while the goal in the analysis of composite materials, is the determination of the effective properties of the homogenized piezoelectric composite which are functions of the electroelastic properties of the constituent phases and the microstructure. In the following sections, the essence of the micromechanic modeling on piezo-composites is described.

2.1. Equations and notations

The constitutive equations for the stationary linear response of a piezoelectric solid can be expressed as

$$\begin{aligned} \varepsilon_{ij} &= S_{ijkl}\sigma_{kl} + g_{kij}D_k \\ (-E_i) &= g_{ijk}\sigma_{jk} - \beta_{ij}D_j \end{aligned} \tag{1}$$

$$\begin{aligned} \sigma_{ij} &= C_{ijmn}\varepsilon_{mn} + e_{nij}(-E_n) \\ (D_i) &= e_{imn}\varepsilon_{mn} - \kappa_{in}(-E_n) \end{aligned} \tag{2}$$

where ε_{ij} is the elastic strain tensor, σ_{ij} the elastic stress tensor, E_i the electric field, (C_{ijmn}, S_{ijkl}) are the elastic stiffness and compliance tensors, and (e_{nij}, g_{ijk}) are the piezoelectric tensors, while (κ_{in}, β_{ij}) are the dielectric tensors. In the above constitutive equations, $(-E_i)$ is used instead of E_i as it will allow the construction of a symmetric generalized linear response matrix. The strain and electric field are derivable from the displacement and electric potential as

$$\varepsilon_{ij} = \tfrac{1}{2}(u_{i,j} + u_{j,i}) \tag{3}$$

$$E_i = -\phi_{,i} \tag{4}$$

In addition, the equations of equilibrium and Gauss' law of electrostatics (in the absence of body forces or free charge) are

$$\sigma_{ij,j} = 0 \tag{5}$$

$$D_{i,i} = 0 \tag{6}$$

In the above equations, conventional indicial notation is utilized where repeated subscripts are summed over the range $1 \rightarrow 3$ and a comma denotes partial differentiation. Eqs. (1) and (2) can be expressed in a concise matrix form

$$\boldsymbol{Z} = \boldsymbol{F}\boldsymbol{\Sigma} \tag{7}$$

$$\boldsymbol{\Sigma} = \boldsymbol{E}\boldsymbol{Z} \tag{8}$$

where variables in bold denote 9×9 matrices ($\boldsymbol{F}$, $\boldsymbol{E}$) or 9×1 column vectors ($\boldsymbol{Z}$, $\boldsymbol{\Sigma}$). The symbolic notation used in Eqs. (7) and (8) is introduced by Barnett and Lothe [20] for electroelastic analysis and further details are given elsewhere [8,9]. The notation is extremely useful as it greatly simplifies the solution procedure of numerous problems in electroelastic analysis, and in particular the numerical

implementation. The matrices in Eqs. (7) and (8) are composed of the following subsets:

$$\boldsymbol{E} = \begin{bmatrix} C_{6\times6} & e^{\mathrm{t}}{}_{(6\times3)} \\ e_{3\times6} & -\kappa_{3\times3} \end{bmatrix}, \qquad \boldsymbol{F} = \begin{bmatrix} S_{6\times6} & g^{\mathrm{t}}{}_{(6\times3)} \\ g_{3\times6} & -\beta_{3\times3} \end{bmatrix} \tag{9}$$

$$\boldsymbol{Z} = \begin{bmatrix} \varepsilon_{(6\times1)} \\ -E_{(3\times1)} \end{bmatrix}, \qquad \boldsymbol{\Sigma} = \begin{bmatrix} \sigma_{(6\times1)} \\ D_{(3\times1)} \end{bmatrix} \tag{10}$$

where the symmetry properties of the moduli [25] have been utilized and a superscript 't' denotes transposition. In Eqs. (9) and (10), the 9×9 matrices $\boldsymbol{E}$ and $\boldsymbol{F}$ are symmetric and are positive definite.

2.2. Effective moduli of piezoelectric composites

The effective electroelastic moduli of two-phase perfectly bonded piezoelectric composites can be derived using the representative volume element (RVE) of the piezoelectric composite [21]. RVE is defined to be a sample, which is structurally representative of the composite body. It contains a sufficiently large number of reinforcing inhomogeneities so that the effective electroelastic moduli are virtually independent of the applied surface loads (traction, displacement, charge, and potential).

Consider that the representative volume element is subjected to homogeneous elastic displacement–electric potential boundary conditions, $\boldsymbol{Z}^0$, i.e. $u_i^0(S) = \varepsilon_{ij}^0 x_j$ and $\phi^0(S)$ where S is its surface. These uniform values can be shown to be equal to the average strain and electric field in the composite [8,9], i.e.

$$\bar{\boldsymbol{Z}} = \frac{1}{V_{\mathrm{D}}}\int_{\mathrm{D}} \boldsymbol{Z}(\boldsymbol{x})\,\mathrm{d}V = \boldsymbol{Z}^0$$

where V_{D} is the volume of the RVE and the dependence of a variable on position is denoted by (x). In a dual manner, when the RVE is subjected to uniform traction and charge boundary conditions, $\boldsymbol{\Sigma}^0$, it is easily shown that $\bar{\boldsymbol{\Sigma}} = \boldsymbol{\Sigma}^0$. These two results are fundamental in the analysis of piezoelectric heterogeneous media. They are a generalization of the widely used average strain and average stress theorems in the elastic behavior of heterogeneous media as forwarded by Hill [21].

The volume-averaged electroelastic fields can be expressed as

$$\bar{\boldsymbol{\Sigma}} = \sum_{i=1}^{N} c_i \bar{\boldsymbol{\Sigma}}_i, \qquad \bar{\boldsymbol{Z}} = \sum_{i=1}^{N} c_i \bar{\boldsymbol{Z}}_i \tag{11}$$

where an overbar denotes the volume average of a quantity. The subscript "i" denotes the ith piezoelectric phase and c_i is the volume fraction of the ith phase. In each phase $\boldsymbol{Z}$ and $\boldsymbol{\Sigma}$ are related through the constitutive Eqs. (7) and (8). The volume-averaged piezoelectric fields are related through the effective electroelastic moduli, $\boldsymbol{E}$ and $\boldsymbol{F}$, i.e.

$$\bar{\boldsymbol{\Sigma}} = \boldsymbol{E}\bar{\boldsymbol{Z}}, \qquad \bar{\boldsymbol{Z}} = \boldsymbol{F}\bar{\boldsymbol{\Sigma}} \tag{12}$$

Use of Eqs. (1)–(4), along with the average field theorems yields explicit equations for the electroelastic moduli:

$$\boldsymbol{E} = \boldsymbol{E}_1 + \sum_{i=1}^{N} c_i(\boldsymbol{E}_i - \boldsymbol{E}_1)\boldsymbol{A}_i \tag{13}$$

$$\boldsymbol{F} = \boldsymbol{F}_1 + \sum_{i=1}^{N} c_i(\boldsymbol{F}_i - \boldsymbol{F}_1)\boldsymbol{B}_i \tag{14}$$

where due to linearity $\boldsymbol{A}_i$ is the *concentration tensor* that relates the average strain and potential gradient ($\boldsymbol{A}_i$) in the ith phase to that in the composite, i.e.

$$\bar{\boldsymbol{Z}}_i = \boldsymbol{A}_i\bar{\boldsymbol{Z}} = \boldsymbol{A}_i\boldsymbol{Z}^0 \tag{15a}$$

Similarily, $\boldsymbol{B}_i$ is the concentration tensor that relates the averaged stress and electric displacement in the ith phase to that in the composite.

$$\bar{\boldsymbol{\Sigma}}_i = \boldsymbol{B}_i\bar{\boldsymbol{\Sigma}} = \boldsymbol{B}_i\boldsymbol{\Sigma}^0 \tag{15b}$$

The concentration tensors satisfy the identities $\sum_{i=1}^{N} c_i\boldsymbol{A}_i = \sum_{i=1}^{N} c_i\boldsymbol{B}_i = \boldsymbol{I}$ where $\boldsymbol{I}$ is the 9×9 identity matrix. The effective moduli in Eqs. (13) and (14) are based on the assumption of perfect alignment of the reinforcing phases with respect to a sample-fixed coordinate system. If this is not the case, the far right-hand term in Eqs. (13) and (14) must be replaced with the orientational average of the quantity, i.e. $\langle(\boldsymbol{E}_i - \boldsymbol{E}_1)\boldsymbol{A}_i\rangle$.

The estimation of the concentration tensors $\boldsymbol{A}_i$ and $\boldsymbol{B}_i$ is the key to predicting the effective electroelastic moduli of a composite, $\boldsymbol{E}$ and $\boldsymbol{F}$. The concentration tensors obtained using the representative volume element of the piezoelectric composite is carried further in the next section to obtain the electroelastic moduli through the use of *micromechanics models*.

2.3. Estimates of concentration tensors

In the following sections, we denote the subscripts 1 and 2 as the matrix and filler phase, respectively.

The simplest approximations of the concentration tensors $\boldsymbol{A}_2$ and $\boldsymbol{B}_2$ are $\boldsymbol{A}_2 = \boldsymbol{I}$ and $\boldsymbol{B}_2 = \boldsymbol{I}$. These are a generalization of the well-known Voigt and Reuss approximations for the elastic moduli of composite materials, respectively. Physically $\boldsymbol{A}_2 = \boldsymbol{I}$ represents the assumption that the strain and electric field are uniform throughout the composite, and $\boldsymbol{B}_2 = \boldsymbol{I}$ represents the assumption that the stress and electric displacement are uniform throughout the composite. These assumptions provide accurate estimates for some components of the effective moduli for some simplified microstructural geometries, e.g. laminates, but are inaccurate in general because they do not take into consideration the shape of the inhomogeneities. A first step to this end is then the dilute approximation. The key assumption made in the dilute approximation is that the interaction among the reinforcing particles in a matrix-based composite can be

ignored. That the composite is assumed to be matrix-based renders the dilute approximation most applicable to 0–3 and 1–3 (in the connectivity terminology of Newham et al. [14]) piezoelectric composites. In these composites, the matrix is connected to itself in three dimensions while the reinforcing phase is self-connected in zero and one dimensions, respectively. For the dilute approximation, the concentration tensors $\boldsymbol{A}_2$ and $\boldsymbol{B}_2$ are obtained from the solution of the auxiliary problem of a single inhomogeneity embedded in an infinite matrix. It is particularly convenient to model the shape of the inhomogeneity as ellipsoidal because this allows us to model a wide range of microstructural geometries. Extreme cases are lamina and continuous fiber-reinforced composites. For an ellipsoidal inhomogeneity the concentration tensor for the dilute case can be expressed as

$$\boldsymbol{A}_2^{\mathrm{dil}} = [\boldsymbol{I} + \boldsymbol{S}\boldsymbol{E}_1^{-1}(\boldsymbol{E}_2 - \boldsymbol{E}_1)]^{-1} \tag{16}$$

where $\boldsymbol{I}$ is the 9×9 identity matrix and $\boldsymbol{S}$ is the 9×9 matrix representation of the Eshelby tensors which are functions only of the shape of the ellipsoid and the electroelastic moduli of the matrix. A brief derivation of Eq. (16) is given in Appendix A, and explicit expressions for $\boldsymbol{S}$ are given by Dunn and Taya [8,9] for elliptical inclusions in transversely isotropic media and Dunn and Wienecke [10] for spheroidal inclusions in transversely isotropic media. A substitution of Eq. (16) into Eq. (12) yields explicit expressions for the dilute predictions of effective electroelastic moduli of piezoelectric composite materials. The expressions are only valid for dilute fiber concentrations (for example, C_2 is less than 0.05) and so their practical application to piezoelectric composites with modest fiber concentrations is limited. As will be seen in the next section, though, this serves as the starting point for the development of theories that are applicable to larger volume fractions. Let us use a more accurate model based on Mori–Tanaka's mean field theory [22].

The key assumption in the Mori–Tanaka [20] theory is that the concentration tensor $\boldsymbol{A}_2$ is given by the solution for a single inhomogeneity embedded in an infinite matrix subjected to the as yet unknown average electroelastic field in the matrix, i.e. $\bar{\boldsymbol{Z}}_2 = \boldsymbol{A}_2^{\mathrm{dil}}\boldsymbol{Z}_1$, where $\boldsymbol{A}_2^{\mathrm{dil}}$ is given by Eq. (16). The concentration tensor based on the Mori–Tanaka theory can then be expressed as

$$\boldsymbol{A}_2^{\mathrm{MT}} = \boldsymbol{A}_2^{\mathrm{dil}}[c_1\boldsymbol{I} + c_2\boldsymbol{A}_2^{\mathrm{dil}}]^{-1} \tag{17}$$

Substituting Eqs. (16) and (17) into Eq. (13) yields explicit expressions for the effective electroelastic moduli of piezoelectric composite materials that are valid for non-dilute filler concentrations. For the case of continuous fiber composite (1–3) or a particulate composite (0–3), the components of the Eshelby tensor $\boldsymbol{S}$ are simple explicit functions. The detailed derivation of Eq. (17) is given as Appendix A.

3. Lamination model

The lamination model was originally developed to analyze the mechanical behavior of a laminated composite plate subjected to thermomechanical loading and its details have been extensively covered in standard textbooks on composites for examples, Gibson [23], and Taya and Arsenault [24].

The analysis of stress field and out-of-plane displacement of rectangular piezoelectric laminates can be obtained by applying electric field through the thickness using the modified classical lamination theory [11,25]. We shall discuss the lamination model, which consists of n layers (laminae) with each lamina having different mechanical and piezoelectric properties. It is noted that the inter-laminar shear stresses cannot be calculated by the CLT. Then more rigorous model based on 2D elasticity [12,26] needs to be used for analysis of the inter-laminar shear stress. However, for the purpose of optimization of the microstructure of laminated piezoelectric composite actuators, use of the CLT is sufficient. Later, we will discuss the difference of the predicted results among various models, CLT, 2D elasticity solutions and FEM.

Consider a laminated plate which consists of n layers with each having different mechanical and piezoelectric properties and is subjected to uniform temperature and constant electric field along the thickness direction (z-direction) as shown in Fig. 1.

The constitutive equations of the ith piezoelectric layer are given in Eq. (2).

Assume that the displacement field along the x- (u), y- (v) and z-direction (w) is defined as

$$\begin{aligned} u(x, y) &= u^0(x, y) + zF_1(x, y) \\ v(x, y) &= v^0(x, y) + zF_2(x, y) \\ w(x, y) &= w^0(x, y) \end{aligned} \tag{18}$$

By using the assumption of transverse shear strain (ε_{xz} and ε_{yz}) are negligible, the strain–displacement relation and Eq. (18), once can obtain [23]

$$F_1(x, y) = -\frac{\partial w}{\partial x} \tag{19a}$$

$$F_2(x, y) = -\frac{\partial w}{\partial y} \tag{19b}$$

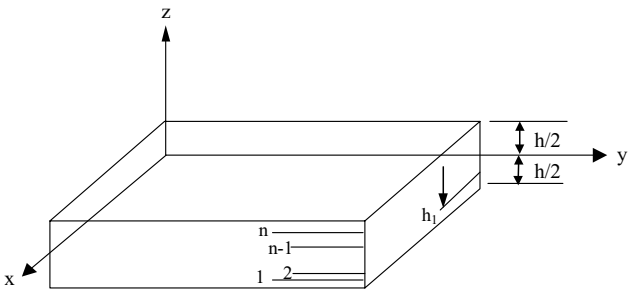

Fig. 1. Laminated composite plate.

From the linear strain–displacement relation, strain ε_{kl} are related to curvatures $\kappa_{ij}(\kappa_x, \kappa_y, \kappa_{xy})$ as

$$\begin{aligned}\varepsilon_x &= \varepsilon_x^0 + z\kappa_x \\ \varepsilon_y &= \varepsilon_y^0 + z\kappa_y \\ \varepsilon_{xy} &= \varepsilon_{xy}^0 + 2z\kappa_{xy}\end{aligned} \tag{20}$$

where u_0, v_0, ε_x^0, ε_y^0, and ε_{xy}^0 are the displacements and strains of the mid-plane of a plate. The in-plane constitutive equations of a piezoelectric material of class 6 mm type can be obtained from Eq. (12) as

$$\begin{Bmatrix}\sigma_x \\ \sigma_y \\ \sigma_{xy}\end{Bmatrix} = \begin{bmatrix}\bar{C}_{11} & \bar{C}_{12} & 0 \\ \bar{C}_{21} & \bar{C}_{22} & 0 \\ 0 & 0 & C_{66}\end{bmatrix}_i \begin{Bmatrix}\varepsilon_x^0 + z\kappa_x \\ \varepsilon_y^0 + z\kappa_y \\ \gamma_{xy}^0 + z\kappa_{xy}\end{Bmatrix} - \begin{bmatrix}0 & 0 & \bar{e}_{31} \\ 0 & 0 & \bar{e}_{32} \\ 0 & 0 & 0\end{bmatrix}_i \begin{Bmatrix}0 \\ 0 \\ E_z\end{Bmatrix}_i \tag{21a}$$

where

$$\bar{C}_{ij} = C_{ij} - \frac{C_{i3}}{C_{33}}C_{j3}, \qquad \bar{e}_{ij} = -\frac{C_{i3}}{C_{33}}e_{33} + e_{ij} \tag{21b}$$

It is noted here that $\bar{C}_{ij}$, $\bar{e}_{ij}$ are the reduced stiffness constants and reduced piezoelectric constants that are modified by the assumption of plane stress and where ε_x^0, ε_y^0, and ε_{xy}^0 are the in-plane strain components at mid-plane, $z = 0$ as shown in Fig. 1, κ_x, κ_y, and κ_{xy} are the curvatures of the plate. The derivation of $\bar{C}_{ij}$ and $\bar{e}_{ij}$ are given in Appendix B. Each piezoelectric lamina is considered a capacitor whose electric field corresponds to its dielectric constant. The electric field in each layer of multi layer FGM piezoelectric material can be obtained by considering the multi layers in a piezoelectric FGM as a series of condensers. The relationship between the electric capacity and the voltage is given as

$$C_t = \frac{Q}{V_t} \tag{22}$$

where C_t is the overall capacitance, Q the charge, and V_t is the total voltage. The total capacitance in a series of capacitance is found as

$$\frac{1}{C_t} = \sum_{i=1}^{n}\frac{1}{C_i} = \sum_{i=1}^{n}\frac{d_i}{\varepsilon_i A} \tag{23}$$

where d_i is the thickness of each capacitance or lamina in the piezoelectric FGM, ε_i the dielectric constant for each lamina and A is the area of the lamina. It is noted here that symbol "ε" was used in a earlier section as "strain tensor", but here it is used "dielectric constant". In Eq. (2), dielectric constant tensor κ_{in} was used, which is now expressed in short as "ε_i" (Nye convention [27]) where subscript i denotes the ith FGM layer (lamina). The electric capacity in each layer will then be

$$C_i = \frac{Q}{V_i} = \frac{\varepsilon_i A}{d_i} \tag{24}$$

From Eqs. (22) to (24), we obtain the electric field in each layer as

$$E_i = \frac{V_i}{d_i} = V_t\frac{1}{\varepsilon_i\sum_{l=1}^{n}(h_l - h_{l-1})/\varepsilon_l} \tag{25}$$

In-plane stress resultants (N_x, N_y, N_{xy}) and stress couples (M_x, M_y, M_{xy}) are defined as

$$\{N, M\} = \sum_{i=1}^{n}\int_{h_{i-1}}^{h_i}\{\sigma\}(\mathrm{d}z, z\,\mathrm{d}z) \tag{26}$$

Substituting Eq. (12) into Eq. (26), we obtain

$$\begin{bmatrix}N \\ M\end{bmatrix} = \begin{bmatrix}A & B \\ B & D\end{bmatrix}\begin{Bmatrix}\varepsilon^0 \\ \kappa\end{Bmatrix} - \begin{bmatrix}N^E \\ M^E\end{bmatrix} \tag{27}$$

where

$$[A, B, D] = \sum_{i=1}^{n}\int_{h_{i-1}}^{h}[\bar{Q}]_i(\mathrm{d}z, z\,\mathrm{d}z, z^2\,\mathrm{d}z) \tag{28a}$$

$$[N, M]^E = \sum_{i=1}^{n}\int_{h_{i-1}}^{h_i}[\bar{e}]_i\{E\}(\mathrm{d}z, z\,\mathrm{d}z) \tag{28b}$$

where $[\bar{Q}]_i$ denotes 3×3 matrix for the ith lamina and given by

$$[\bar{Q}]_i = \begin{bmatrix}\bar{Q}_{11} & \bar{Q}_{12} & 0 \\ \bar{Q}_{12} & \bar{Q}_{22} & 0 \\ 0 & 0 & Q_{66}\end{bmatrix} \tag{28c}$$

$$\bar{Q}_{ij} = C_{ij} - \frac{C_{i3}C_{j3}}{C_{32}} \tag{28d}$$

$$Q_{66} = C_{66} \tag{28e}$$

In the above derivation, we assumed that the piezoelectric laminated plate is subjected to an applied electric field which is distributed in each layer in the laminate based on the dielectric constant of the layer as formulated in Eqs. (22)–(25). Under the applied electric field ($E_x = E_y = 0$, $E_z \neq 0$) in the absence of applied mechanical loading, we obtain from Eq. (26) the strain of the mid-plane strain curvature as

$$\begin{bmatrix}\varepsilon^0 \\ \kappa\end{bmatrix} = \begin{bmatrix}a & b \\ b & d\end{bmatrix}\begin{bmatrix}N^E \\ M^E\end{bmatrix} \tag{29}$$

where

$$\begin{bmatrix}a & b \\ b & d\end{bmatrix} = \begin{bmatrix}A & B \\ B & D\end{bmatrix}^{-1} \tag{30}$$

Under a given electric field throughout the laminate, one can then predict the stress and displacement field of each layer as well as the out-of-plane displacement of the laminate plate.

Table 1
Mechanical and piezoelectric properties

Material	C_{11} (GPa)	C_{12} (GPa)	C_{13} (GPa)	C_{33} (GPa)	C_{44} (GPa)	e_{31} (C/m^2)	e_{33} (C/m^2)	e_{15} (C/m^2)	d_{31} (10^{-12} m/v)	d_{33} (10^{-12} m/v)	d_{15} (10^{-12} m/v)	$\varepsilon_{33}/\varepsilon_0$[a]
PZT-C91	120	77	77	114	24	−17.3	21.2	20.2	−340	645	841	2664
PZT-C6	123	77	80	112	19	−7.3	17.2	14.5	−229	480	763	749
PZT-C3	148.5	77.4	79.2	135.5	32.5	−1.21	11.03	9.48	−59	152	292	338
Platinum	70	30	30	70	33	0	0	0	0	0	0	–

[a] ε_0 (C/(N m^2)) = 8.85 × 10^{-12}.

4. Calculation of electroelastic properties of each lamina predicted by the Eshelby's method

The electroelastic properties of each lamina of a laminated composite are predicted using the micromechanic model discussed in Section 2. The electroelastic properties of the constituent piezoelectric materials that are used in this study are shown in Table 1. Three piezoelectric materials are investigated, PZT-C91, PZT-C6, and PZT-C3 which are commercially available from Fuji Ceramics Corporation, Japan, therefore PZT-C91, PZT-C3, and PZT-C6 are piezoceramics based on PZT that are actually used in processing piezo-actuators of both standard bimorph and FGM bimorph types (see Section 6). Among these PZT piezoceramics PZT-C91 exhibits the maximum piezoelectric properties while PZT-C3 exhibits the minimum piezoelectric properties. Two types of piezoelectric composites are investigated, C6-C91 and C3-C91. PZT-C91 was chosen as the parent (matrix) material of the composite while PZT-C6 and PZT-C3 are used as fillers. The elastic constant C_{11}, piezoelectric contact e_{33} and dielectric constant ε_{33} of the composite as predicted by the micromechanic model are shown as a function of the filler V_f, in Figs. 2–4, respectively. The elastic, piezoelectric, and dielectric properties have been observed to vary in a fairly linear manner. This is due to the small difference in the electroelastic properties among the three different PZT materials used here. If there exists a large difference in the properties, the relation between the electroelastic properties and the volume fraction of discontinuous filler is expected to become non-linear.

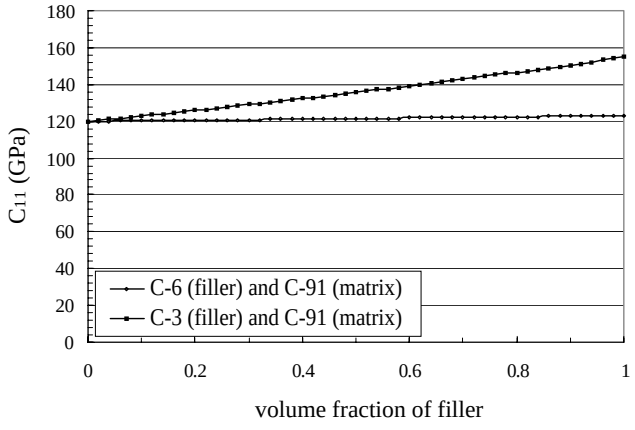

Fig. 2. Elastic properties of piezoelectric composites.

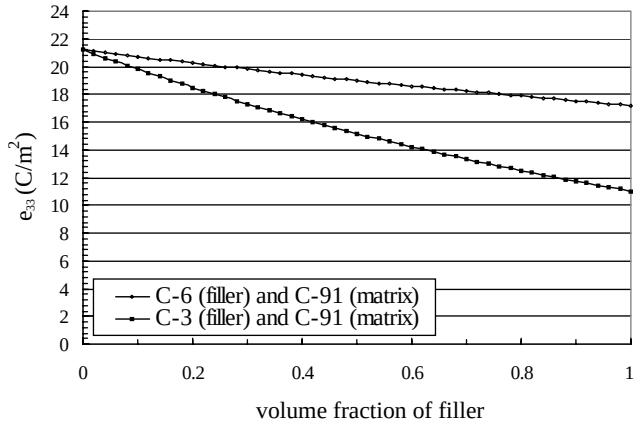

Fig. 3. Piezoelectric properties of piezoelectric composites.

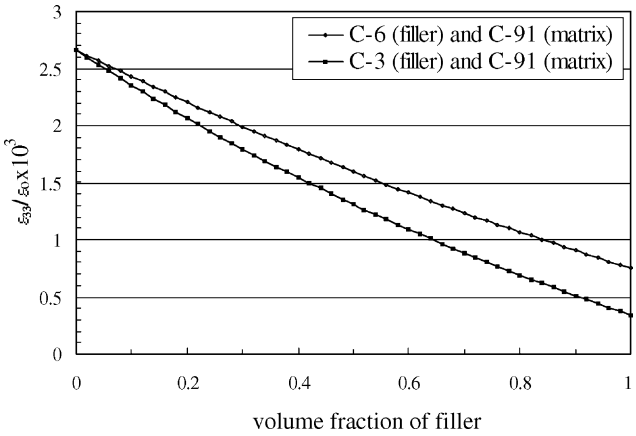

Fig. 4. Dielectric properties of piezoelectric composite.

5. Design and optimization of piezo laminated composite actuators

A standard bimorph actuator consists of top and bottom layers with identical electroelastic properties but opposite electric polarity as shown in Fig. 5(a). Upon an applied electric field, the top layer (lamina) extends while the bottom shrinks, resulting in bending with convex upward, but this induces a large misfit in the in-plane strain between the

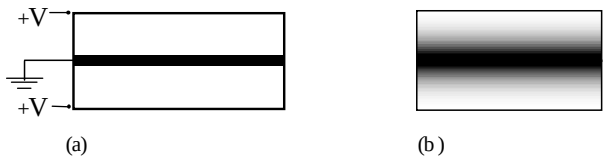

Fig. 5. Piezoelectric actuators: (a) standard bimorph and (b) FGM bimorph.

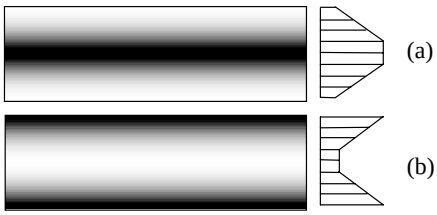

Fig. 6. Piezoelectric properties distribution in FGM bimorph (a) type A and (b) type B.

top and bottom laminae with possible premature failure of the interface under an increasing electric field. The concept of functionally graded microstructure is thus applied to the piezoelectric actuator plate for a bending mode as shown in Fig. 5(b) with aim of reducing the misfit strain between laminae. One can consider two types of grading through the laminate thickness, type A where the piezoelectric properties increases toward the mid-plane, and type B where piezoelectric properties decrease toward the mid-plane (Fig. 6).

The laminated composite plate investigated is of 50 mm length, 0.67 mm thickness subjected to applied voltage in the *z*-direction of 33 V (average electric field is 100 V/mm). The thickness of the top and bottom piezoelectric layers in the standard bimorph is 0.33 mm and the thickness of the platinum electrode located in the middle of the laminate is 0.01 mm. In the standard bimorph case, three piezoelectric systems are investigated to obtain the best system in terms of maximum out-of-plane displacement and minimum stress field as shown in Table 2. PZT-C91 exhibits the maximum displacement and maximum stress while C6 exhibits a relatively high displacement with moderate stresses. The C3 piezo-material has the lowest piezoelectric properties (see Table 1) and does not exhibit a good performance in terms of out-of-plane displacement. Next,

Table 2
Maximum in-plane stresses and bending deflection of three standard bimorph actuators

	Standard bimorph system		
	C91	C6	C3
Applied voltage (V)	33	33	33
Laminate thickness (mm)	0.67	0.67	0.67
No. of layers	2	2	2
Layer thickness (mm) (Pt = 0.01)	0.33	0.33	0.33
Electric field (V/mm)	100	100	100
Curvature (m^{-1})	0.152	0.102	0.026
Maximum σ_x (MPa)	3.08	1.9	0.75
Deflection (μm) for plate length 50 mm	47.5	31.9	8.0

the FGM bimorph actuators of type A and type B are considered. The dimension of the FGM bimorph actuators is 50 mm long and 20 mm wide and 0.67 mm thick. Each FGM layer (or lamina) is 0.11 mm thick while the middle layer is a platinum plate with 0.01 mm thick. The effects of the number of layers on the best performance of the FGM actuator is examined, although only two cases, i.e. 6 and 10 layers FGM. This is constrained by the processing. The normal stress, σ_x, and out-of-plane displacement, w, of the FGM bimorph piezoelectric laminate plate are calculated using the classical lamination model theory, where the plate is simply supported and subjected to average electric field of 100 V/mm across the thickness, and the mid-plane electrode is platinum for the case of FGM bimorph of types A and B, respectively. The results based on CLT modeling are given in Tables 3 and 4. By comparing the results of standard bimorph (Table 2), the FGM bimorph of type A (Table 3) and of type B (Table 4), we can conclude that the FGM bimorph of type B whose electroelastic properties decrease toward the mid-plane, exhibits modest performance despite its low stress level. In the FGM bimorph of type A, the case of 6 layers FGM shows better performance than 10 layers FGM as shown in Table 3. In other words, the use of type A FGM bimorph with six layers where the piezoelectric properties increases toward the middle of the laminate has shown the best performance in terms of reduction in normal stress, σ_x, while maintaining a relatively high bending displacement of 43.6 μm. As to

Table 3
Comparison of bending displacement for type A piezo-composite FGM bimorph

	FGM bimorph system (type A FGM microstructure)			
	C91–C6	C91–C3	C91–C6	C91–C3
Applied voltage (V)	33	33	33	33
Laminate thickness (mm)	0.67	0.67	0.67	0.67
No. of layers	6	6	10	10
Layer thickness (mm) (Pt = 0.01)	0.11	0.11	0.066	0.066
Electric field (V/mm)	100	100	100	100
Curvature (m^{-1})	0.14	0.048	0.141	0.054
Maximum σ_x (MPa)	1.48	0.87	1.59	1.05
Bending displacement (μm) for plate length 50 mm	43.6	15.0	43.9	16.9

Table 4
Comparison of bending displacement for type B piezo-composite FGM bimorph

	FGM bimorph system (type B FGM microstructure)			
	C91–C6	C91–C3	C91–C6	C91–C3
Applied voltage (V)	33	33	33	33
Laminate thickness (mm)	0.67	0.67	0.67	0.67
No. of layers	6	6	10	10
Layer thickness (mm) (Pt = 0.01)	0.11	0.11	0.066	0.066
Electric field (V/mm)	100	100	100	100
Curvature (m^{-1})	0.093	0.04	0.097	0.05
Maximum σ_x (MPa)	3.38	1.6	3.63	1.99
Bending displacement (μm) for plate length 50 mm	29.2	14.1	30.5	16.2

Table 5
Comparison of bending displacement and in-plane stress σ_x in various types of piezo-composite plates

	Type of FGM microstructure			
	Standard bimorph		Bimorph FGM	
	C91	C6	C91–C6 type A	C91–C6 type B
Applied voltage (V)	33	33	33	33
Laminate thickness (mm)	0.67	0.67	0.67	0.67
No. of layers	2	2	6	6
Layer thickness (mm) (Pt = 0.01)	0.33	0.33	0.11	0.11
Electric field (V/mm)	100	100	100	100
Curvature (m^{-1})	0.152	0.102	0.143	0.094
Maximum σ_x (MPa)	3.08	1.91	1.48	3.38
Bending displacement (μm) for plate length 50 mm	47.5	31.9	43.6	29.2

the normal stress in the FGM bimorph of type A, σ_x, is estimated as 1.48 MPa which is 50% less than that in the case of C91 standard bimorph, 3.08 MPa. It is noted in Table 3 that the FGM bimorph of type A using the C91–C3 composite exhibits a poor performance in bending displacement compared to the C91–C6 piezoelectric composite although the former exhibited the lowest stress. The best performance cases of standard bimorph, FGM bimorph of types A and B are summarized in Table 5, where the number of FGM layers for the FGM bimorph actuators is chosen as 6. It can be concluded from Table 5 that the case of the FGM bimorph of type A provides the best overall performance, i.e. minimizing the induced stress field while achieving high bending displacement.

For the purpose of optimum design of piezolaminated composite actuator under requirements of large bending displacement and smaller stress field, we used CLT model which can provide us with in-plane stress σ_x, but not interlamina shear stress τ_{xz} (see Fig. 1). The shear stress τ_{xz} is considered to be responsible for dilamination from side surface as the magnitude of τ_{xz} is the maximum at free-end and decreases toward the mid-center. The calculation of τ_{xz} requires use of the 2D elasticity model [12] and finite element method. Table 6 summarizes the experimental results of bending displacement and the predicted results of bending displacement and stress field (σ_x and τ_{xz}). Table 6 supports the validity of CLT model as compared with the experimental results and the predictions by more rigorous model of 2D elasticity [12] and FEM. It also supports the notion that the larger the values of σ_x, the larger the values of τ_{xz}. Therefore, we used in our optimization analysis the values of σ_x predicted by CLT model.

The effects of the distribution of the piezoelectric properties in the FGM bimorph are next investigated. The distribution of the volume fraction of filler phase, V_f, is chosen

Table 6
Comparison of ANSYS FEM results with the analytical values for piezo-actuators, standard bimorph EGM bimorph tapes A and B

Bimorph system	Maximum bending displacement (μm)	Maximum (MPa)	
		σ_x	τ_{xz}
Standard bimorph			
Experimental	49.6	–	–
CLT	47.5	3.08	–
2D elasticity	47.8	3.07	1.48
FEM	47.6	3.17	1.56
FGM bimorph type A			
Experimental	43.8	–	–
CLT	43.6	1.48	–
2D elasticity	44.9	1.63	0.59
FEM	44.8	1.65	0.63
FGM bimorph type B			
Experimental	30.4	–	–
CLT	29.2	3.38	–
2D elasticity	29.5	3.69	1.82
FEM	29.4	3.75	1.9

as follows:

$$V_f = \left(\frac{i-1}{n-1}\right)^{1/m} \tag{31}$$

where i is the ith layer, n the number of layers in the laminate and, m the FGM volume fraction exponent. It is noted that exponent m governs the distribution pattern of the electroelastic properties across the thickness of the FGM laminated composite. If $m = 1$, the distribution is linear. By manipulating the FGM volume fraction exponent, the performance of the actuator can be enhanced in terms of stress field and out-of-plane displacement. To this end, we use the 6 layer FGM bimorph of type A as it has similar performance to the 10 layered FGM bimorph, and also due to the easiness of fabrication compared to the 10 layered FGM bimorph. The stress field and out-of-plane displacements are calculated by CLT and the results are plotted as a function of the FGM volume fraction exponent, m are in Figs. 6 and 7, respectively. The bending displacement has increased slightly with m compared to the linear distribution, while the stress has a slight reduction from the linear distribution. It can be concluded from Figs. 7 and 8 that the FGM layer distribution exponent has modest influence on the out-of-plane displacement and in-plane stress field, justifying use of linear distribution ($m = 1$), which we use in processing of the FGM bimorph actuators.

Further optimization of the FGM bimorph is carried out, focusing on the effect of thickness of FGM layers in the C91–C6 type A FGM bimorph on the bending displacement

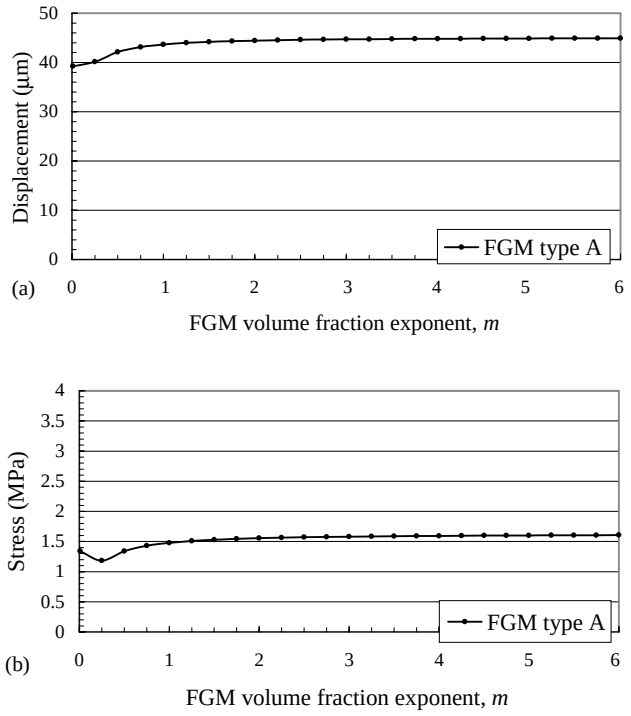

Fig. 7. Out-of-plane displacement (a) and in-plane stress (b) field for type A FGM bimorph vs. FGM volume fraction exponent under 100 V/mm average electric field.

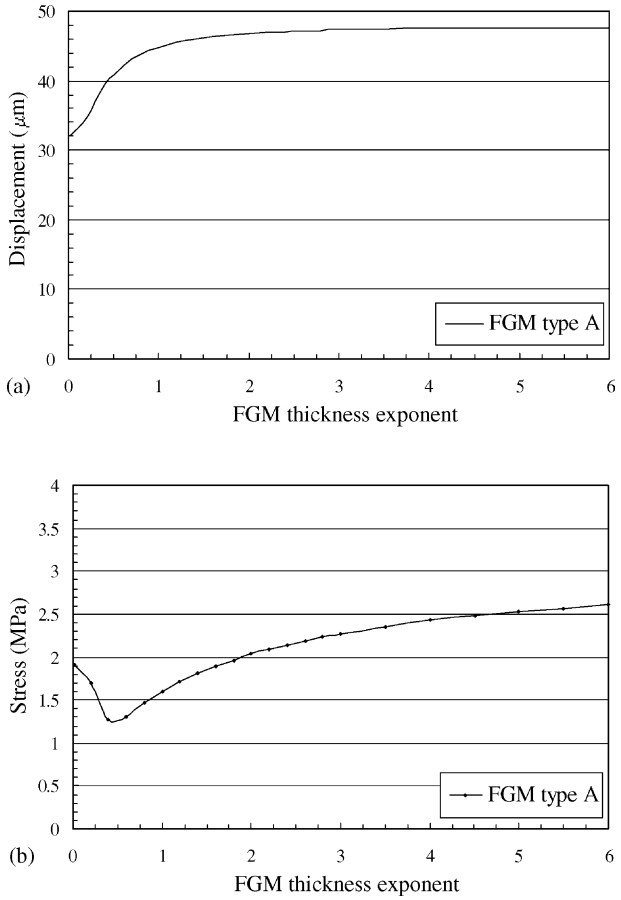

Fig. 8. The out-of-plane displacement (a) and in-plane stress (b) field vs. the FGM thickness exponent under 100 V/mm applied average electric field.

and in-plane stress maximum stress σ_x of the FGM bimorph type A actuator. The thickness of each layer is chosen according to the following equation:

$$\frac{h_i - \sum_{l=1}^{i} h_{l-1}}{h_t} = \left(\frac{i}{n}\right)^{1/p} \tag{32}$$

where h_i and h_t are the thickness of the ith layer and the total thickness of the laminate, n the number of layers in the laminate, p is the FGM thickness exponent. The results predicted by CLT of the FGM-bimorph type A actuator are shown in Fig. 8. The bending displacement increases sharply with the increase of the FGM thickness exponent until the FGM thickness exponent reaches one, then the displacement stabilizes and increases slightly. The minimization of the maximum σ_x can be achieved when the FGM thickness exponent, p, reaches 0.5. The in-plane stress increases steadily with the increase in the FGM thickness exponent, p. Since there is no single value of p which provides the maximum bending displacement and minimum in-plane stress and the effect of p is found modest, we shall use $p = 1$ from now on in our design. Therefore, from the results of Figs. 7 and 8, we take both FGM volume fraction parameter m and thickness exponent p as 1. The predicted results of the bending

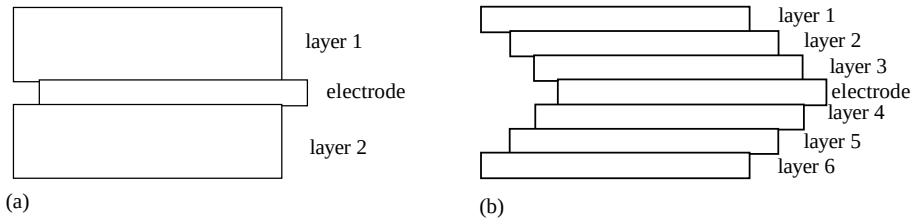

Fig. 9. Illustration of thickness profile of piezo-actuators (a) standard biomorph and (b) FGM biomorph.

displacement and maximum in-plane stress σ_x of the FGM piezo-actuators are obtained with $m = p = 1$, as shown in Table 5.

6. Experimental results of piezoelectric actuators

Two different types of piezo-actuator plates were prepared; standard bimorph, FGM bimorph of types A and B (see Figs. 5 and 6). The temperature of specimens was raised from room temperature to the sintering temperature of 1200 °C at the rate of 100 °C/h, maintained for 30 min and then cooled at the same rate as the rising phase. After sputtered gold electrodes were applied on both surfaces, specimens were poled in a silicone bath with a dc field of 2 kV/mm at 170 °C for 30 min, and then cooled down to 50 °C in the field. The rectangular piezoelectric plate is 50 mm long, 20 mm wide, and 0.67 mm thick. The standard bimorph consists of two piezoelectric layers of 0.33 thickness separated by a thin platinum electrode of 0.01 mm thickness as in Fig. 9(a). The FGM bimorph consists of six layers of 0.11 mm with the mid-layer being a 0.01 mm thick platinum electrode (Fig. 9(b)). The piezo-actuators were processed using the tape casting technique, where each piezoelectric composite lamina was made into a green tape of thickness 0.13 mm at sending speed of 1 m/min. The binder used was methyl cellulose, which was removed under 750 °C for 5 h. The shrinkage of each lamina after the de-bindering process was about 0.5% across the thickness direction. Weight (2 g) was placed on the top of laminated sheets that were de-bindered, during the sintering process. The advantage of using tape casting is that no epoxy is needed to bond the different piezoelectric layers since the actuator is sintered as a whole. The actuator is then electroded and poled for testing. The out-of-plane displacements of the piezo-actuator are measured using laser displacement measurement system (LDMS), which measures the difference between the reflected rays before and after actuation, which provides the displacement of a piezo-actuator. Under increasing applied voltage, out-of-plane displacements are measured by LDMS. The measured out-of-plane (bending) displacements of standard bimorph, FGM bimorph of types A and B actuators are plotted in symbols in Fig. 10 where the predictions by the CLT are also shown for comparison.

7. Conclusion

Bimorph piezo-composite actuators with functionally graded microstructure are designed by using several analytical models. The analytical model is hierarchical, consisting of micromechanic model based on Eshelby's type model for each lamina and laminated composite plate model. Based on the predictions, the optimum FGM associated with bimorph

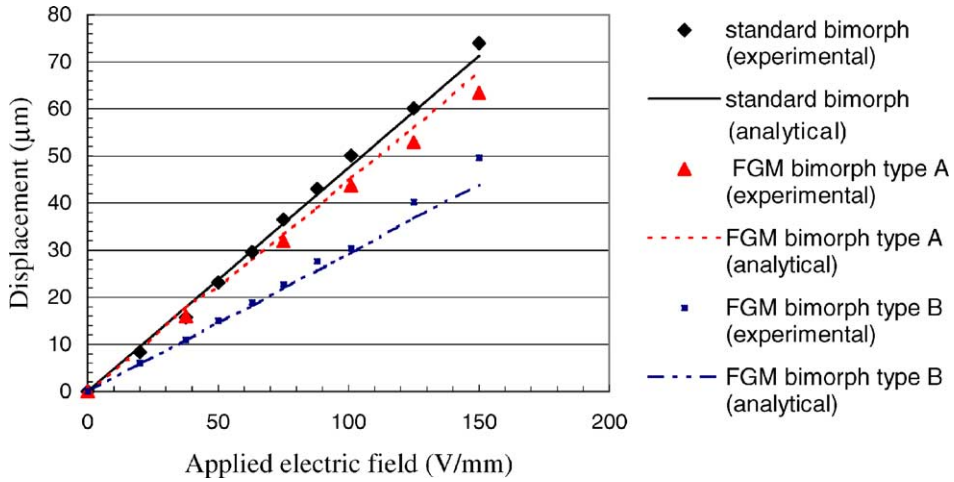

Fig. 10. Bending displacement vs. applied electric field, experimental data and predictions by CLT model of several types of piezo-composite actuators.

actuator is determined with aim of maximizing bending displacement and minimizing the induced stress field. The bimorph piezo-composite actuator with FGM type A where the electroelastic properties increase toward the mid-plane was found to exhibit large bending displacement and least induced stress field, therefore it is the best design (Fig. 10). The measured bending displacements of the bimorph FGM actuator and standard bimorph actuator are compared with the predictions by the models, resulting in a good agreement.

Acknowledgements

This research was supported by a grant from AFOSR (F49620-02-1-0028) and also by a contract from NEDO on Smart Materials and Structure via RIMCOF, Japan.

Appendix A. A concentration matrix A

A.1. Dilute case

Consider a piezoelectric composite consisting of n infinite domain (D) containing an ellipsoidal particle (inhomogeneity). The ellipsoidal particle is of the same shape and aligned with the a_3, principal axis coincident with the χ_3 axis. The piezoelectric particle (Ω) has electroelastic moduli $\boldsymbol{E}_2$ while the matrix, D–Ω, has electroelastic module $\boldsymbol{E}_1$. The composite is subjected to the far-field applied stress and electric displacement $\boldsymbol{\Sigma}^0$. Using the equivalent inclusion method for piezoelectric composites [6,7] the stress and electric displacement in the representative particles can be written as

$$\boldsymbol{\Sigma} = \boldsymbol{E}_2[\boldsymbol{Z}^0 + \boldsymbol{Z}] = E_1[\boldsymbol{Z}^0 + \boldsymbol{Z} - \boldsymbol{Z}^*], \tag{A.1}$$

where $\boldsymbol{Z}$ represents the perturbation of the strain and electric fields in the particle with respect to those in the matrix and $\boldsymbol{Z}^*$ is the fictitious eigenfield required to ensure that the equivalency of Eq. (A.1) holds. In Eq. (A.1), $\boldsymbol{Z}$ and $\boldsymbol{Z}^*$ are related through

$$\boldsymbol{Z} = \boldsymbol{S}\boldsymbol{Z}^* \tag{A.2}$$

where $\boldsymbol{S}$ is the coupled electroelastic analog of Eshelby's tensor and is defined explicitly in the paper by Dunn and Taya [8]. The strain and potential gradient in the inclusion (which are uniform) are given by

$$\boldsymbol{Z}_2 = \boldsymbol{Z}^0 + \boldsymbol{S}\boldsymbol{Z}^* \tag{A.3}$$

With Eqs. (A.1) and (A.3), $\boldsymbol{Z}_2$ can be obtained as

$$\left\lfloor \boldsymbol{I} + S\boldsymbol{E}_1^{-1}(\boldsymbol{E}_2 - \boldsymbol{E}_1) \right\rfloor \boldsymbol{Z}_2 = \boldsymbol{Z}^0 \tag{A.4}$$

From Eqs. (A.4) and (20), $\boldsymbol{A}^{\mathrm{dil}}$ is given by

$$\boldsymbol{A}^{\mathrm{dil}} = [\boldsymbol{I} + \boldsymbol{S}\boldsymbol{E}_1^{-1}(\boldsymbol{E}_2 - \boldsymbol{E}_1)]^{-1} \tag{A.5}$$

A.2. Mori–Tanaka mean field theory

When the volume fraction of fillers becomes large, the interactions among fillers cannot be ignored. Let us first consider the field vector $\boldsymbol{Z}_0$ prescribed on the composite boundary, where numerous ellipsoidal fillers are embedded in the matrix. Now we insert an ellipsoidal filler into the average field in the matrix with $\boldsymbol{Z}_1$. Then using the solution of the dilute case, the field vector in any representative filler $\boldsymbol{Z}_2$ is related to $\boldsymbol{Z}_0$, $\boldsymbol{Z}_1$

$$\boldsymbol{Z}_{\mathrm{f}} = \boldsymbol{A}^{\mathrm{dil}}\boldsymbol{Z}_1 \tag{A.6}$$

where $\boldsymbol{A}^{\mathrm{dil}}$ is given by Eq. (A.5).

If the Mori–Tanaka theory is valid, $\boldsymbol{Z}_2$ is also related to the applied field vector $\boldsymbol{Z}_0$, then

$$\boldsymbol{Z}_2 = \boldsymbol{A}^{\mathrm{MT}}\boldsymbol{Z}_0 \tag{A.7}$$

where $\boldsymbol{A}^{\mathrm{MT}}$ is the concentration tensor by the Mori–Tanaka theory.

From Eqs. (11) and (A.6),

$$\begin{aligned}\boldsymbol{Z}_0 &= (1-f)\boldsymbol{Z}_1 + f\boldsymbol{Z}_2 = (1-f)\boldsymbol{Z}_1 + f(\boldsymbol{A}^{\mathrm{dil}}\boldsymbol{Z}_1)\\ &= [(1-f) + f\boldsymbol{A}^{\mathrm{dil}}]\boldsymbol{Z}_1\end{aligned} \tag{A.8}$$

where f is the volume fraction of fillers.

From Eq. (A.6)

$$\boldsymbol{Z}_1 = (\boldsymbol{A}^{\mathrm{dil}})^{-1}(\boldsymbol{Z}_2) \tag{A.9}$$

Eliminating $\mathbf{Z}_1$ from Eqs. (A.8) and (A.9)

$$\boldsymbol{Z}_0 = \left\lfloor (1-f)\boldsymbol{A}^{\mathrm{dil}} + f\boldsymbol{I} \right\rfloor \boldsymbol{Z}_{\mathrm{f}} \tag{A.10}$$

Solving for $\boldsymbol{Z}_2$, we obtain

$$\boldsymbol{Z}_2 = [(1-f)(\boldsymbol{A}^{\mathrm{dil}})^{-1} + f\boldsymbol{I}]^{-1}\boldsymbol{Z}_0 \tag{A.11}$$

comparison between Eqs. (A.7) and (A.11) yields

$$\begin{aligned}\boldsymbol{A}^{\mathrm{MT}} &= [(1-f)(\boldsymbol{A}^{\mathrm{dil}})^{-1} + f\boldsymbol{I}]^{-1}\boldsymbol{Z}_0\\ &= \boldsymbol{A}^{\mathrm{dil}}[(1-f)\boldsymbol{I} + f\boldsymbol{A}^{\mathrm{dil}}]^{-1}\end{aligned} \tag{A.12}$$

where $\boldsymbol{A}^{\mathrm{dil}}$ is given by Eq. (A.5).

In the above equations, we have removed subscript '2' from $\boldsymbol{A}^{\mathrm{dil}}$ to avoid crowdedness in the expressions. It is noted that phase '2' is the same as filler phase, 'f', but as volume fraction increases, the difference between matrix ('1') phase and filler ('2') phase is reduced. Therefore, the Mori–Tanaka theory can be applied to higher volume fractions.

Appendix B. Reduced stiffness and piezoelectric properties for plane stress

The constitutive equations of a piezoelectric material, under applied electric field, E_z only, are expressed as

$$\begin{Bmatrix}\sigma_x\\ \sigma_y\\ \sigma_z\\ \sigma_{yz}\\ \sigma_{xz}\\ \sigma_{xy}\end{Bmatrix} = \begin{bmatrix} C_{11} & C_{12} & C_{13} & & & \\ & C_{22} & C_{23} & & 0 & \\ & & C_{33} & & & \\ & & & C_{44} & & \\ & \text{sym.} & & & C_{55} & \\ & & & & & C_{66}\end{bmatrix} \begin{Bmatrix}\varepsilon_x\\ \varepsilon_y\\ \varepsilon_z\\ \varepsilon_{yz}\\ \varepsilon_{xz}\\ \varepsilon_{xy}\end{Bmatrix} - \begin{bmatrix} 0 & 0 & e_{13}\\ 0 & 0 & e_{23}\\ 0 & 0 & e_{33}\\ 0 & e_{24} & 0\\ e_{15} & 0 & 0\\ 0 & 0 & 0\end{bmatrix} \begin{Bmatrix}0\\ 0\\ E_z\end{Bmatrix} \tag{B.1}$$

The assumption of plane stress in z-axis, where $\sigma_z = \sigma_{xz} = \sigma_{yz} = 0$, leads to

$$\sigma_z = C_{13}\varepsilon_x + C_{23}\varepsilon_y + C_{33}\varepsilon_z - \varepsilon_{33}E_z = 0 \tag{B.2}$$

The strain in the z-axis then becomes

$$\varepsilon_z = \frac{1}{C_{33}}(-C_{13}\varepsilon_x - C_{23}\varepsilon_y + \varepsilon_{33}E_z) \tag{B.3}$$

By substituting Eq. (B.3) into Eq. (B.1), the constitutive equations of a piezoelectric material under the applied electric field, and under the assumption of plane stress in z-axis, are reduced to

$$\begin{Bmatrix}\sigma_x\\ \sigma_y\\ \sigma_{xy}\end{Bmatrix} = \begin{bmatrix} C_{11} - \frac{C_{13}}{C_{33}}C_{13} & C_{12} - \frac{C_{13}}{C_{33}}C_{23} & 0\\ C_{12} - \frac{C_{13}}{C_{33}}C_{23} & C_{22} - \frac{C_{13}}{C_{33}}C_{23} & 0\\ 0 & 0 & C_{66}\end{bmatrix} \times \begin{Bmatrix}\varepsilon_x\\ \varepsilon_y^0\\ \gamma_{xy}^0\end{Bmatrix} - \begin{bmatrix} 0 & 0 & -\frac{C_{13}}{C_{33}}e_{33} + e_{13}\\ 0 & 0 & -\frac{C_{13}}{C_{33}}e_{33} + e_{23}\\ 0 & 0 & 0\end{bmatrix} \begin{Bmatrix}0\\ 0\\ E_z\end{Bmatrix} \tag{B.4}$$

Eq. (B.4) can be simplified as presented in Eq. (21a) and (21b).

References

[1] K. Uchino, M. Yoshizaki, K. Kasai, K. Yamamura, N. Sakai, H. Asakura, Jpn. J. Appl. Phys. 26 (1987) 1046.
[2] G.H. Haertling, Am. Ceram. Soc. Bull. 73 (1994) 93.
[3] C.C. Wu, M. Khau, W. May, J. Am. Ceram. Soc. 79 (1996) 809.
[4] C. Gamano, IEEE Trans. Audio Electron. 19 (1970) 6.
[5] K. Uchino, Acta Mater. 46 (1998) 3745.
[6] X. Zhu, Z. Meng, Sens. Actuators A48 (1995) 169.
[7] X. Zhu, J. Xu, Z. Meng, J. Xhu, S. Zhou, Q. Li, Z. Liu, N. Ming, Mater. Design 21 (2000) 561.
[8] M.L. Dunn, M. Taya, Proc. R. Soc. London A443 (1993) 265.
[9] M.L. Dunn, M. Taya, Int. J. Solids Struct. 30 (1993) 161.
[10] M.L. Dunn, H.A. Wienecke, Int. J. Solids Struct. 34 (1997) 3571.
[11] A.A. Almajid, M. Taya, S. Hudnut, Int. J. Solids Struct. 38 (2001) 3377.
[12] A.A. Almajid, M. Taya, J. Int. Mater. Syst. Struct. 12 (2001) 341.
[13] W.A. Smith, Proc. IEEE Ultrasonics Symp. 755 (1989).
[14] R.E. Newham, D.P. Skinner, L.E. Cross, Mater. Res. Bull. 13 (1978) 525.
[15] K.A. Klicker, J.V. Biggers, R.E. Newham, J. Am. Ceram. Soc. 64 (1) (1981) 5.
[16] W.A. Smith, A.A. Shaulov, B.A. Auld, Proc. IEEE Ultrasonics Symp. 642 (1985).
[17] W.A. Smith, Proc. IEEE Ultrasonics Symp. 757 (1990).
[18] W.A. Smith, B.A. Auld, IEEE Trans. Ultrason. Ferroelectr. Frequency Control 38 (1) (1991) 40.
[19] W.A. Smith, IEEE Trans. Ultrason. Ferroelectr. Frequency Control 40 (1993) 41.
[20] D.M. Barnett, J. Lothe, Phys. Stat. Sol. (b) 67 (1975) 105.
[21] R. Hill, J. Mech. Phys. Solids 11 (1963) 357.
[22] T. Mori, K. Tanaka, Acta Metall. 21 (1973) 571.
[23] R.F. Gibson, Principles of Composite Material Mechanics, McGraw-Hill, New York, 1994.
[24] M. Taya, R.J. Arsenault, Metal Matrix Composites: Thermomechanical Behavior, Pergamon Press, New York, 1989.
[25] W. Sun, Proc. Smart Struct. Int. Syst. SPIE 1917 (1993) 497.
[26] D.C. Lagondas, B. Zhonghe, Smart Mater. Struct. 3 (1994) 309.
[27] J.F. Nye, Physical Properties of Crystals, Oxford University Press, Oxford, 1957.

Biographies

Minoru Taya obtained his BS in engineering in 1968 from University of Tokyo, and his MS in 1973 and PhD 1977 in theoretical applied mechanics from Northwestern University. Dr. Taya is currently professor of mechanical engineering, adjunct professor of materials science and engineering, and also electrical engineering, at University of Washinnton. Dr. Taya stayed at University of Oxford as a senior guest research fellow of Royal Society of London during 1986. During the period of 1989–1991, he served as professor of materials systems, Tohoku University, Department of Materials Processing. Dr. Taya is currently running a Center for Intelligent Materials and Systems as director, where he is involved in supervising a number of projects related to intelligent materials and systems. The intelligent materials are shape memory alloys (SMA), ferromagnetic SMA, piezo-composites, electro- and photo-active polymers. Dr. Taya is also involved in designing devices based on these intelligent materials.

Abdulhakim Almajid received his PhD in mechanical engineering from the University of Washington at Seattle in 2002. Currently, he is an assistant professor of the Mechanical Engineering Department at King Saud University in Saudi Arabia. His research lies in the smart materials and MEMS technologies, design and processing of piezoelectric devices. His research applications include microelectronics, transducers.

Martin L. Dunn is currently a professor of mechanical engineering at the University of Colorado at Boulder. He received the PhD in mechanical engineering from the University of Washington in 1992 and was a postdoctoral appointee at Sandia National Laboratories. His research focuses on the micromechanical behavior of materials and structures. He has pub-

lished over 75 articles in archival journals in these areas, and his research has been sponsored by NSF, DOE, NIST, DARPA, AFOSR, and Sandia National Laboratories.

H. Takahashi received his MS in electronics, Shizuoka University in 1992. He started working for Fuji Ceramics Corporation, where he is the manager of Research and Development Department in electronic ceramics. Mr. Takahashi has been working on a new processing route based on micro-wave sintering and hot-press to process a set of new high performance piezoceramic materials, which include the PZT system, and the PNN–PZT composite system to achieve higher piezoelectric data of these ceramics.